PAPER

Magnetic and magnetocaloric properties of an unusual family of carbonate-panelled [Ln$_6^{III}$Zn$_2^{II}$] cages†

Waqas Sethi,[a,b] Sergio Sanz,[b] Kasper S. Pedersen,[a] Mikkel A. Sørensen,[a] Gary S. Nichol,[b] Giulia Lorusso,[c] Marco Evangelisti,*[c] Euan K. Brechin*[a] and Stergios Piligkos*[a]

The reaction of the pro-ligand H$_4$L, which combines the complementary phenolic oxime and diethanol-amine moieties within the same organic framework, with Zn(NO$_3$)$_2$·6H$_2$O and Ln(NO$_3$)$_3$·6H$_2$O in a basic methanolic solution generates a family of isostructural heterometallic coordination compounds of general formula [Ln$_6$Zn$_2$(CO$_3$)$_5$(OH)(H$_2$L)$_4$(H$_3$L)$_2$(H$_4$L)]NO$_3$·xMeOH [Ln = Gd, x = 30 (**1**), Ln = Dy, x = 32 (**2**), Ln = Sm, x = 31 (**3**), Ln = Eu, x = 29 (**4**), Ln = Tb, x = 30 (**5**)]. The octametallic skeleton of the cage describes a heavily distorted [Gd$_6^{III}$] octahedron capped on two faces by Zn^{II} ions. The metal core is stabilised by a series of μ$_3$- and μ$_4$-CO$_3^{2-}$ ions, originating from the serendipitous fixation of atmospheric CO$_2$. The magnetic properties of all family members were examined *via* SQUID magnetometry, with the χ$_M$T product and VTVB data of the Gd analogue (**1**) being independently fitted by numerical diagonalisation to afford the same best-fit parameter J$_{Gd-Gd}$ = −0.004 cm^{-1}. The MCE of complex **1** was elucidated from specific heat data, with the magnetic entropy change reaching a value of 22.6 J kg^{-1} K^{-1} at T = 1.7 K, close to the maximum entropy value per mole expected from six Gd^{III} spins (S$_{Gd}$ = 7/2), 23.7 J kg^{-1} K^{-1}.

Introduction

The large value of their total angular momentum, their often strong magnetic anisotropy and the inherently weak magnetic exchange mediated *via* their contracted f-orbitals engender Ln-based molecular cages with some fascinating and potentially useful low temperature physics.[1–5] In academia these have been much exploited for the construction of Single-Molecule Magnets (SMMs)[6] and Molecular Coolers.[7] The prospect of employing molecular cages in low temperature cooling applications is based upon the compounds magneto-caloric effect (MCE), as derived from the change in magnetic entropy upon application of a magnetic field.[8] The design of such molecular materials therefore requires the control and optimi-

sation of quantum properties at the molecular level (spin ground state, magnetic anisotropy, the presence of low-lying excited spin states), which in turn requires the synthetic chemist to follow a particular recipe that includes high spin, anisotropic metal ions and lightweight organic bridging ligands.[9]

When a magnetic field is applied to a polynuclear molecular magnetic material in which the magnetic exchange interaction between constitutive metal centres and the local magnetic anisotropies are small, the magnetic moments of the constitutive paramagnetic centres become polarised by the magnetic field. When this magnetisation process is performed at constant temperature, the total magnetic entropy of the material is reduced. In a subsequent adiabatic demagnetisation process, the temperature of the material decreases, thereby cooling the material.[10] This is a particularly attractive, and potentially technologically important phenomenon, since recent studies have shown that the MCE of some molecular clusters can be much larger than that found in the best inter-metallic and lanthanide alloys, and magnetic nanoparticles employed commercially.[11,12] The obvious metal ion of choice is Gd^{III} since it possesses an isotropic S = 7/2, and its clusters will exhibit weak magnetic exchange courtesy of the contracted f-orbitals, resulting in the presence of field-accessible, low-lying excited states. Indeed the vast majority of clusters

[a]Department of Chemistry, University of Copenhagen, Universitetsparken 5, 2100, Denmark. E-mail: piligkos@kiku.dk
[b]EaStCHEM School of Chemistry, The University of Edinburgh, David Brewster Road, Edinburgh, Scotland EH9 3FJ, UK. E-mail: ebrechin@staffmail.ed.ac.uk
[c]Instituto de Ciencia de Materiales de Aragón y Departamento de Física de la Materia Condensada, CSIC-Universidad de Zaragoza, 50009 Zaragoza, Spain. E-mail: evange@unizar.es
†Electronic supplementary information (ESI) available: Crystallographic data in tabulated format, and additional structural and magnetic figures. CCDC 1055091–1055095. For ESI and crystallographic data in CIF or other electronic format see DOI: 10.1039/c5dt01240f
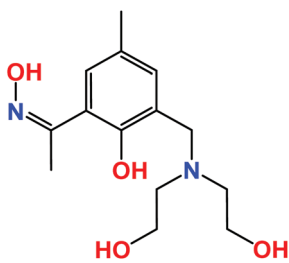
Scheme 1 The structure of the ligand H$_4$L which contains both phenolic oxime and diethanolamine moieties.

reported recently to display an enhanced MCE have contained multiple Gd^{III} centres.[13–18] We continue this trend by reporting the syntheses, structures, magnetic and magnetocaloric properties of a rather unusual set of complexes of general formula [Ln$_6$Zn$_2$(CO$_3$)$_5$(OH)(H$_2$L)$_4$(H$_3$L)$_2$(H$_4$L)]NO$_3$·xMeOH [Ln = Gd, x = 30 (**1**), Ln = Dy, x = 32 (**2**), Ln = Sm, x = 31 (**3**), Ln = Eu, x = 29 (**4**), Ln = Tb, x = 30 (**5**)] built with the ligand (Z)-1-(3-((bis(2-hydroxyethyl)aminomethyl)-2-hydroxy-5-methylphenyl)ethan-1-one oxime), [H$_4$L], shown in Scheme 1. We have previously shown that this ligand is highly effective in forming transition metal cages with aesthetically pleasing structures and fascinating magnetic properties, and we now extend its coordination chemistry to the 4f elements.[19]

Experimental

Materials and physical measurements

All manipulations were performed under aerobic conditions, using materials as received (reagent grade). (Z)-1-(3-((Bis(2-hydroxyethyl)aminomethyl)-2-hydroxy-5-methylphenyl)ethan-1-one oxime) [H$_4$L] was synthesised as described in the literature.[19] Magnetisation data were acquired on a MPMS-XL SQUID magnetometer equipped with a 5 T dc magnet. Freshly isolated crystalline material was covered immediately with hexadecane (MP = 18 °C) in order to suppress loss of co-crystallized solvent. Dc susceptibility data were obtained with H_{dc} = 1000 Oe in the temperature range 1.8–280 K and magnetisation data at $H_{dc} \leq$ 50 kOe at selected low temperatures. All data were corrected for diamagnetic contributions from the sample, hexadecane and the capsule by means of Pascals constants. Specific heat measurements were carried out at temperatures down to 0.3 K by using a Quantum Design 9T-PPMS, equipped with a ^{3}He cryostat. The experiments were performed on thin pressed pellets (ca. 1 mg) of a polycrystalline sample, thermalised by ca. 0.2 mg of Apiezon N grease, whose contribution was subtracted using a phenomenological expression.

Syntheses

General synthetic procedure for complexes **1–3**: Ln(NO$_3$)$_3$·xH$_2$O (0.25 mmol), Zn(NO$_3$)$_2$·6H$_2$O (75 mg, 0.25 mmol), H$_4$L (140 mg, 0.5 mmol), ^{t}BuONa (100 mg, 1 mmol) and Et$_3$N (300 μL, 2.15 mmol) were stirred in 25 ml MeOH for 2 hours.

The solution was then filtered and allowed to stand. X-ray quality crystals formed *via* slow evaporation of the mother liquor over a period of 5 days in ∼30–40% yield. Complex **4** was made in the same manner, but using 0.5 mmol (100 mg) ^{t}BuONa, whilst no ^{t}BuONa was added to the reaction mixture to make **5**. Elemental analyses, calculated (found): **1**: C 36.18 (36.24), H 4.27 (4.61), N 6.14 (6.19). **2**: C 35.85 (34.97), H 4.24 (4.52), N 6.09 (5.81). **3**: C 36.62 (35.40), H 4.33 (4.28), N 6.22 (5.92). **4**: C 36.52 (35.36), H 4.31 (4.38), N 6.20 (5.73). **5**: C 36.07 (34.91), H 4.26 (4.42), N 6.13 (5.95).

X-ray crystallography

Diffraction data were collected on a Bruker Smart Apex CCD diffractometer equipped with an Oxford Cryosystems LT device, using Mo radiation. Data collection parameters and structure solution and refinement details are listed in Table S1.† Full details can be found in the CIF files provided in the ESI† and CCDC 1055091–1055095.

Results and discussion

Compounds **1–5** are isostructural, and so for the sake of brevity we limit discussion to complex **1**, [Gd$_6^{III}$Zn$_2^{II}$(CO$_3$)$_5$(OH)(H$_2$L)$_4$(H$_3$L)$_2$(H$_4$L)]NO$_3$·30MeOH (Fig. 1). The metallic skeleton of the cage describes a highly distorted [Gd$_6^{III}$] octahedron with the two Zn^{II} ions each capping a triangular face. The core of the molecule is stabilised by the presence of five CO$_3^{2-}$ ions, originating from the serendipitous fixation of atmospheric CO$_2$. These exhibit several different bonding modes [μ$_3$-Gd$_3$, μ$_3$-Gd$_2$Zn, μ$_3$-Gd$_4$, μ$_4$-Gd$_4$, μ$_4$-Gd$_2$Zn$_2$] as shown in Fig. 1B. There is a single $^-$OH ion which μ-bridges between Gd4 and Gd6 (Gd–O–Gd, 112°) and four H$_2$L^{2-}, two H$_3$L$^-$ and one H$_4$L ligands that adorn the outer periphery of the molecule. These
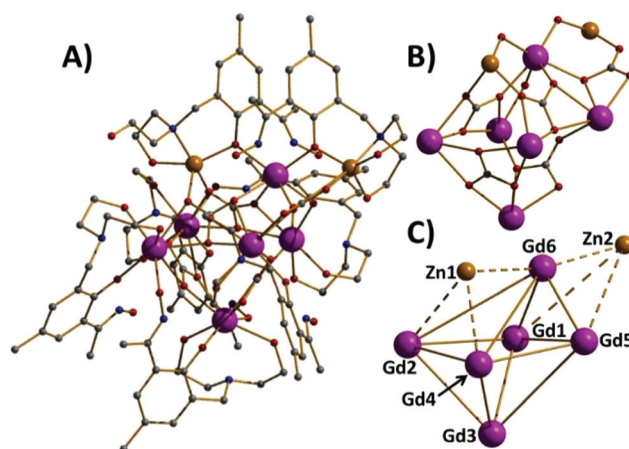
Fig. 1 (A) The structure of the cation of complex **1**. (B) The metal core highlighting the role of the bridging carbonate ions. (C) The metal skeleton of the cage emphasising the highly distorted Gd octahedron and two face-capping Zn ions. Colour code: Gd = purple, Zn = gold, O = red, N = blue, C = grey. H atoms, the nitrate counter ion and solvent molecules of crystallisation are omitted for clarity.
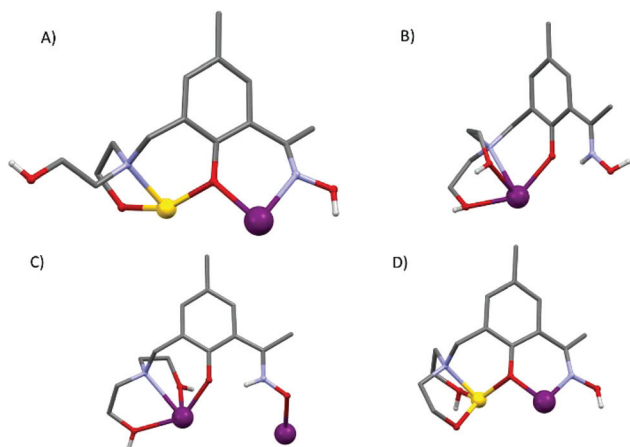
Fig. 2 The different bonding modes of the H_2L^{2-}, H_3L^- and H_4L ligands highlighting the diverse levels of protonation.

ligands exhibit four different coordination modes as shown in Fig. 2: the majority bond in a μ-fashion along the edges of the Gd octahedron, or between a Gd vertex and a Zn cap. One ligand (H_4L) chelates Gd5 through its phenolic and alkoxide O-atoms, with its oximic O- and N-atoms remaining non-coordinating, and H-bonding to the alkoxide O-atom on a neighbouring ligand (O···O, ~2.6 Å). Indeed all of the organic ligands are involved in extensive intramolecular H-bonding interactions with their neighbouring ligands and to the MeOH molecules of crystallisation (Fig. S2 and 3†). All of the Gd ions are nine coordinate $\{GdO_8N\}$ and in capped square anti-prismatic geometries, with the exception of Gd6 which is eight coordinate $\{GdO_6N_2\}$ and square antiprismatic; the latter being the only Ln ion that is not chelated by the diethanolamine moieties. The Zn ions are both five coordinate $\{ZnO_4N\}$ and in distorted trigonal bipyramidal geometries.

There are several close intermolecular contacts. The diethanolamine O-atoms coordinated to Zn2 are H-bonding to the equivalent group on their nearest neighbour (O···O, 2.46 Å; Zn···Zn, 4.14 Å), and at the opposite end of the molecule the Ph rings of the organic ligands are involved in π···π stacking interactions (C···C, 3.58 Å). The result is the formation of a serpentine-like H-bonded chain of cationic cages (Fig. S3†). Closest contacts between these chains are through the Me-groups on the Ph rings of the organic ligand and between the same moiety and the –CH$_2$ arms of the diethanolamine unit (Me···CH$_3$/CH$_2$, ~4 Å). This produces 2D sheets of cations of **1** forming an overall layered structure in the crystal (Fig. S3†). The presence of the carbonate ligands is intriguing, and one that is becoming ever more prevalent with the increasing number of Ln-based cages being reported. Of the ~130 entries in the CSD of metal cluster compounds containing carbonate anions approximately ~25% are 4f complexes and ~5% are heterometallic 3d–4f complexes.[20] While the majority have been formed serendipitously, this observation has led some researchers to deliberately employ Na_2CO_3, $NaHCO_3$ and CO_2 as reaction ingredients.[21] The CSD search also highlights the

extraordinary coordinative flexibility of the CO_3^{2-} ion demonstrating bridging modes ranging from bidentate to non-adentate – with the majority (65%) being tridentate and forming M_3 triangles, a topology of inherent interest to the magnetochemist.[22]

Magnetic properties

The d.c. molar magnetic susceptibility, χ_M, of polycrystalline samples of complexes **1–5** were measured in an applied magnetic field, B, of 0.1 T, over the 2–280 K temperature, T, range. The experimental results are shown in Fig. 3 in the form of χ_MT products, where $\chi = M/B$, and M is the magnetisation of the sample. At room temperature, the χ_MT products of **1–5** have values of 47.2, 84.1, 0.3, 8.9 and 71.3 cm^3 K mol^{-1}, respectively. These are in good agreement with the sum of Curie constants for a $[Gd_6^{III}]$ unit (47.3 cm^3 K mol^{-1}, $g_{Gd} = 2.0$) for **1**, a $[Dy_6^{III}]$ unit (85.0 cm^3 K mol^{-1}, $g_{Dy} = 4/3$) for **2**, a $[Sm_6^{III}]$ unit (0.5 cm^3 K mol^{-1}, $g_{Sm} = 2/7$) for **3**, and a $[Tb_6^{III}]$ unit (70.9 cm^3 K mol^{-1}, $g_{Tb} = 3/2$) for **5**. In the case of **4**, although the $^7F_0$ ground state of Eu^{III} possesses no magnetic moment and thus the $[Eu_6^{III}]$
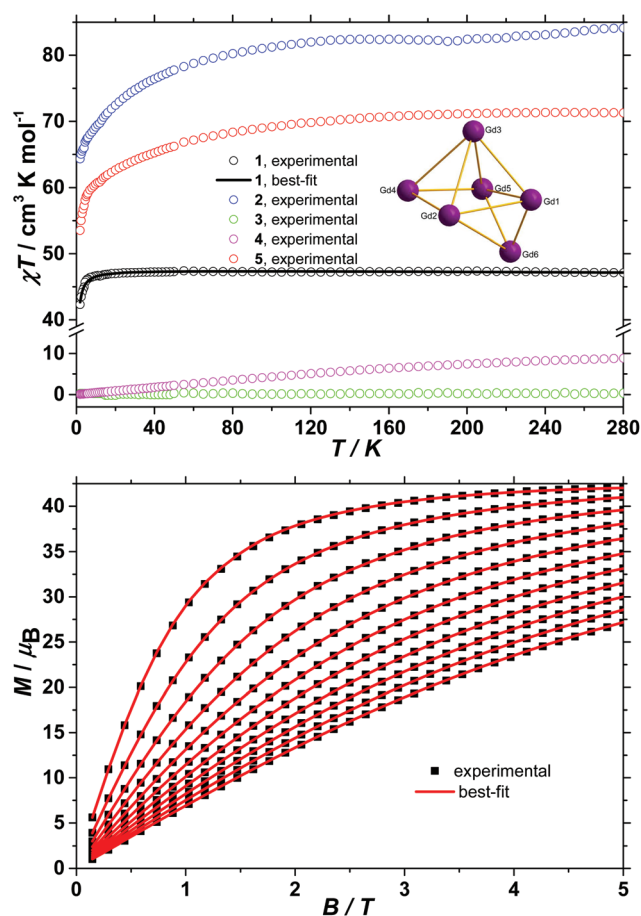

Fig. 3 (Top) Temperature dependence of the χ_MT product of polycrystalline samples of **1–5** with B = 0.1 T. The inset shows the magnetic exchange pathways in the Gd$_6$ unit. The low-temperature field-dependence of the magnetisation of **1**.

unit should be diamagnetic at low temperatures, a finite magnetic moment is observed at room temperature, due to the low-lying $^7F_1$ first excited state that is partly populated at room temperature. Upon cooling, the $\chi_M T$ product of **1** remains essentially constant down to approximately 20 K, wherefrom it begins to decrease upon further cooling to reach 42.3 cm^3 K mol^{-1} at 2 K. Given that the anisotropy of Gd^{III} is negligible, this behaviour is consistent with the presence of weak intramolecular antiferromagnetic exchange interactions. The $\chi_M T$ products of **2** and **5** decrease continuously upon cooling, reaching 64.3 and 53.5 cm^3 K mol^{-1}, respectively, at 2 K. This behaviour can be ascribed to the large magnetic anisotropy of Dy^{III} and Tb^{III} and potentially to the presence of weak intramolecular magnetic exchange interactions. The $\chi_M T$ product of **3** remains essentially constant in the investigated temperature range, at the low, but finite value of 0.3 cm^3 K mol^{-1}, a consequence of the low Landé g-factor of the ground $^6H_{5/2}$ term, indicating a splitting between the ground and first excited Kramers doublets of the $^6H_{5/2}$ term larger than the thermal energy at 280 K. Finally, the $\chi_M T$ product of **4** decreases continuously upon cooling and reaches virtually zero at 2 K, reflecting the thermal depopulation of the $^7F_1$ first excited state upon cooling, likely indicating mixing of the $^7F_0$ ground state with excited states possessing a magnetic moment. To better define the low-temperature magnetic properties of complexes **1–5**, low temperature variable-temperature-and-variable-field (VTVB) magnetisation data were measured in the temperature and magnetic field ranges 2 to 12 K and 0 to 5 T for **1** and **2**, to 8 K and 0 to 5 T for the remaining complexes. The VTVB magnetisation data of **1** are shown in Fig. 3. At the highest investigated field (5 T) and the lowest investigated temperature (2 K), the magnetisation of **1** is 42.1μ_B (μ_B is the Bohr magneton), thus 7.0μ_B per Gd^{III} and in good agreement with the expected (7.0μ_B, for g_{Gd} = 2.0). This is consistent with the presence of very weak exchange interactions operating in **1**. Furthermore, when the VTVB data of **1** are plotted against the reduced quantity $\mu_B B/kT$ (Fig. S4†), no nesting of the VTVB data is observed. This indicates that the energy spectrum of **1** does not present significant splitting with respect to the temperature of measurement at zero magnetic field.

The VTVB magnetisation data of **2** to **5** are shown in Fig. S5–S8,† respectively. At the highest investigated field (5 T) and the lowest investigated temperature (2 K), the magnetisation of **2** and **5** is 32.0 and 29.4μ_B, respectively, thus 5.3 and 4.9μ_B per Dy^{III} and Tb^{III}, respectively. These values are significantly lower than the expected magnetic moment of isolated Dy^{III} (10.0μ_B) and Tb^{III} (9.0μ_B) centres, for which the $m_J = -15/2$ projection of the $^6H_{15/2}$ ground term or the $m_J = -6$ projection of the $^7F_6$ ground term, respectively, is the lowest energy state. Furthermore, the VTVB data of **2** (Fig. S5†) and **5** (Fig. S8†) present nesting when plotted against $\mu_B B/kT$. These observations indicate that the energy spectra of **2** and **5** present significant splittings with respect to the temperature of measurement, at zero magnetic field. The VTVB magnetisation data of **3** (Fig. S6†) present no nesting when plotted against

the reduced quantity $\mu_B B/kT$ and are also linear with magnetic field. This behaviour is consistent with the presence of a thermally isolated Kramers doublet as the ground state of the $^6H_{5/2}$ ground term, in agreement with the analysis of the temperature dependence of the $\chi_M T$ product. Finally, the VTVB magnetisation data of **4** (Fig. S7†) responds in a linear fashion with magnetic field and constant temperature, and are temperature independent at a constant field. This behaviour indicates a field-induced mixing of the $^7F_0$ ground state with excited states possessing a magnetic moment, consistent with the analysis of the temperature dependence of the $\chi_M T$ product.

The hexanuclear nature of complexes **2–5**, combined with the low symmetry of the local coordination sphere of the Ln^{III} centres and the ensuing large number (twenty-seven) of associated ligand field parameters per Ln^{III} ion, precludes any quantitative interpretation of the magnetic properties of these complexes. However, in the case of **1**, given that the orbital angular moment for Gd^{III} is quenched, a quantitative analysis is possible through the use of a spin-Hamiltonian parameterisation. Thus, we employed the general form of the isotropic spin-Hamiltonian (1)

$$\hat{H} = \mu_B B \sum_i g_i \hat{S}_i - 2 \sum_{i,j<i} J_{ij} \hat{S}_i \cdot \hat{S}_j \qquad (1)$$

where the summation indexes i, j run through the constitutive Gd^{III} centres, $\hat{S}$ is a spin operator and J is the isotropic exchange interaction parameter. In our spin-Hamiltonian model we include the following isotropic exchange parameters: $J_{12}, J_{13}, J_{15}, J_{16}, J_{23}, J_{24}, J_{26}, J_{34}, J_{35}, J_{45}, J_{56}$ (Fig. 3, top, inset) and set them all equal to J_{Gd-Gd}. Furthermore we fix $g_{Gd} = 2.0$. Thus our model contains only one free parameter, namely J_{Gd-Gd}. The $\chi_M T$ product and VTVB data of **1** were independently fitted to spin-Hamiltonian (1) by numerical diagonalization and by use of the Levenberg–Marquardt algorithm.[23] Both fits result in the same best-fit parameter: $J_{Gd-Gd} = -0.004$ cm^{-1}. The best-fit curves are shown as solid lines in Fig. 3.

Next, we report the specific heat (C) data collected for a polycrystalline sample of **1** in the temperature range 0.3 to 30 K and in applied magnetic fields, B, of 0, 1, 3 and 7 T (Fig. 4). At the higher temperatures, the specific heat is dominated by a nonmagnetic contribution arising from thermal vibrations of the lattice, which can be modelled by the Debye–Einstein model (dotted line).[8] The phonon specific heat simplifies to a $C/R = aT^3$ dependence at the lowest temperatures, where R is the gas constant and $a = 1.1 \times 10^{-2}$ K^{-3}. For $B \geq 1$ T, we model the field-dependent specific heat as the sum of the Schottky curves arising from the field-split levels of Gd^{III} independent spins (solid lines). Note the nice overall agreement agreement with the experimental data, suggesting that applied fields of $B \geq 1$ T are nearly sufficient for fully decoupling the spin centres. The zero-applied-field specific heat can be described by the Schottky curve depicted in Fig. 4 as a dashed line. This curve is calculated by assuming that every spin centre is experiencing an effective field $B_{eff} = 0.25$ T, as the result of the magnetic interactions involved. By making use of
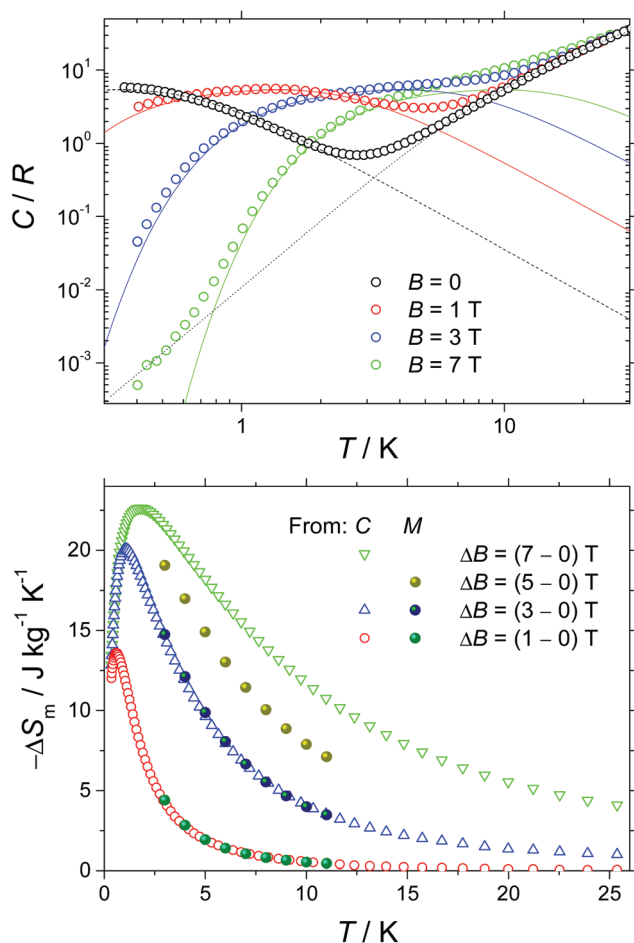
Fig. 4 (Top) Molar specific heat *vs.* *T* for the labelled applied magnetic fields. Solid and dotted lines are, respectively, the Schottky and lattice contributions, calculated as explained in the text. Dashed line is the Schottky contribution, as obtained for an effective B_{eff} = 0.25 T. (Bottom) Temperature dependence of the magnetic entropy change for the indicated magnetic field changes. Data are obtained from specific heat (empty markers) and magnetisation (full markers) experiments.

six Gd^{III} spins (S_{Gd} = 7/2), calculated as $6R\ln(2\,S_{Gd} + 1)$ = 103.7 J mol^{-1} K^{-1}, that is, 23.7 J kg^{-1} K^{-1}. Thus, in **1**, nearly the full magnetocaloric potential of Gd^{III} is achieved.

Conclusions

A highly unusual family of Ln_6Zn_2 cages whose structures are based on highly distorted bicapped octahedra can be constructed from the simple one-pot self-assembly reaction between the two metal salts and the ligand H_4L in basic methanolic solutions. The ligand has been previously used in Mn coordination chemistry to produce dodecametallic wheels and truncated tetrahedra. Magnetic exchange between the Gd^{III} ions in the octahedron is shown to be vanishingly small by independent fits of both susceptibility and magnetisation data. The MCE of complex **1** was elucidated from specific heat data, with the magnetic entropy change reaching a value of 22.6 J kg^{-1} K^{-1} at T = 1.7 K, close to the maximum entropy value per mole expected from six Gd^{III} spins, 23.7 J kg^{-1} K^{-1}.

Acknowledgements

Notes and references

1 J. D. Rinehart and J. R. Long, *Chem. Sci.*, 2011, **2**, 2078.
2 D. N. Woodruff, R. E. P. Winpenny and R. A. Layfield, *Chem. Rev.*, 2013, **113**, 5110.
3 R. Sessoli and A. K. Powell, *Coord. Chem. Rev.*, 2009, **253**, 2328.
4 L. Sorace, C. Benelli and D. Gatteschi, *Chem. Soc. Rev.*, 2011, **40**, 3092.
5 *Lanthanides and Actinides in Molecular Magnetism*, ed. R. A. Layfield and M. Murugesu, Wiley VCH, 2015.
6 E. K. Brechin and G. Aromí, *Struct. Bonding*, 2006, **1**, 1; C. J. Milios and R. E. P. Winpenny, *Struct. Bonding*, 2015, **164**, 1.
7 M. Evangelisti, in *Molecular Magnets, NanoScience and Technology*, ed. J. Bartolomé, F. Luis and J. F. Fernández, Springer, Berlin, 2014, pp. 365–387.
8 M. Evangelisti, F. Luis, L. J. de Jongh and M. Affronte, *J. Mater. Chem.*, 2006, **16**, 2534.
9 M. Evangelisti and E. K. Brechin, *Dalton Trans.*, 2010, **39**, 4672.
10 J. W. Sharples and D. Collison, *Polyhedron*, 2013, **54**, 91.
11 M. Evangelisti, A. Candini, A. Ghirri, M. Affronte, E. K. Brechin and E. J. L. McInnes, *Appl. Phys. Lett.*, 2005, **87**, 072504; R. Shaw, R. H. Laye, L. F. Jones, D. M. Low, C. Talbot-Eeckelaers, Q. Wei, C. J. Milios, S. Teat, M. Helliwell, J. Raftery, M. Evangelisti, M. Affronte,

the specific heat data, we calculate the entropy (S) according to the expression $S/R = \int C/T \mathrm{d}T$, which we plot in Fig. S10† as a function of temperature and for the corresponding applied field values. The final step in the evaluation of the MCE of **1** consists of obtaining the magnetic entropy change $-\Delta S_m(T)$, for selected applied field changes ΔB. The result is shown in Fig. 4. This calculation is straightforwardly obtained from the $S(T)$ curves in Fig. S10† and also from the magnetisation data in Fig. 3 by employing the Maxwell relation, $\Delta S_m = \int \partial M/\partial T \mathrm{d}B$. As can be seen in Fig. 4, the nice agreement between the results obtained *via* both methods is validation of the approaches employed. For the largest applied field change (ΔB = 7 T), the magnetic entropy change, $-\Delta S_m$, reaches 22.6 J kg^{-1} K^{-1} at T = 1.7 K. Because of the very weak strength of the magnetic exchange interactions, this value of $-\Delta S_m$ is close to the maximum entropy value per mole involved, corresponding to

D. Collison, E. K. Brechin and E. J. L. McInnes, *Inorg. Chem.*, 2007, **46**, 4968.

12 M. Manoli, R. D. L. Johnstone, S. Parsons, M. Murrie, M. Affronte, M. Evangelisti and E. K. Brechin, *Angew. Chem., Int. Ed.*, 2007, **46**, 4456; M. Manoli, A. Collins, S. Parsons, A. Candini, M. Evangelisti and E. K. Brechin, *J. Am. Chem. Soc.*, 2008, **130**, 11129.

13 G. Karotsis, M. Evangelisti, S. J. Dalgarno and E. K. Brechin, *Angew. Chem., Int. Ed.*, 2009, **48**, 9928; G. Karotsis, S. Kennedy, S. J. Teat, C. M. Beavers, D. A. Fowler, J. J. Morales, M. Evangelisti, S. J. Dalgarno and E. K. Brechin, *J. Am. Chem. Soc.*, 2010, **132**, 12983.

14 K. S. Pedersen, G. Lorusso, J. J. Morales, T. Weyhermüller, S. Piligkos, S. K. Singh, D. Larsen, M. Schau-Magnussen, G. Rajaraman, M. Evangelisti and J. Bendix, *Angew. Chem., Int. Ed.*, 2014, **53**, 2394.

15 M. Evangelisti, O. Roubeau, E. Palacios, A. Camón, T. N. Hooper, E. K. Brechin and J. J. Alonso, *Angew. Chem., Int. Ed.*, 2011, **50**, 6606.

16 S. K. Langley, N. F. Chilton, B. Moubaraki, T. Hooper, E. K. Brechin, M. Evangelisti and K. S. Murray, *Chem. Sci.*, 2011, **2**, 1166.

17 J. W. Sharples, D. Collison, E. J. L. McInnes, J. Schnack, E. Palacios and M. Evangelsiti, *Nat. Commun.*, 2014, **5**, 5321; J. W. Sharples, Y.-Z. Zheng, F. Tuna, E. J. L. McInnes and D. Collison, *Chem. Commun.*, 2011, **47**, 7650.

18 G. Lorusso, J. W. Sharples, E. Palacios, O. Roubeau, E. K. Brechin, R. Sessoli, A. Rossin, F. Tuna, E. J. L. McInnes, D. Collison and M. Evangelisti, *Adv. Mater.*, 2013, **25**, 4653.

19 S. Sanz, J. M. Frost, M. B. Pitak, S. J. Coles, S. Piligkos, P. J. Lusby and E. K. Brechin, *Chem. Commun.*, 2014, **50**, 3310; J. M. Frost, S. Sanz, T. Rajeshkumar, M. B. Pitak, S. J. Coles, G. Rajaraman, W. Wernsdorfer, J. Schnack, P. J. Lusby and E. K. Brechin, *Dalton Trans.*, 2014, **43**, 10690.

20 See for example: J. B. Peng, Q. C. Zhang, X. J. Kong, Y. Z. Zheng, Y. P. Ren, L. S. Long, R. B. Huang, L. S. Zheng and Z. Zheng, *J. Am. Chem. Soc.*, 2012, **134**, 3314.

21 See for example: Y. N. Guo, X. H. Chen, S. Xue and J. Tang, *Inorg. Chem.*, 2012, **51**, 4035; T. N. Hooper, R. Inglis, M. A. Palacios, G. S. Nichol, M. B. Pitak, S. J. Coles, G. Lorusso, M. Evangelisti and E. K. Brechin, *Chem. Commun.*, 2014, **50**, 3498.

22 J. Schnack, *Dalton Trans.*, 2010, **39**, 4677.

23 W. H. Press, S. A. Teukolsky, W. T. Vetterling and B. P. Flannery, *Numerical recipes in C: The Art of Scientific Computing*, Cambridge University Press, Cambridge, 2nd edn, 1992.